PRAMANA
— journal of
physics

Vol. 65, No. 5
November 2005
pp. 841–846

Ferromagnetic resonance investigation of nanocrystalline FeCuNbSiB

G A BASHEED and S N KAUL
School of Physics, University of Hyderabad, Hyderabad 500 046, India
E-mail: kaulsp@uohyd.ernet.in; kaul_sn@yahoo.com

Abstract. An elaborate line-shape analysis of the ferromagnetic resonance (FMR) spectra taken in the temperature range 100 K to 350 K on amorphous FeCuNbSiB alloys before and after nanocrystallizing them reveals that in the nanocrystalline state, (i) spin wave stiffness (D) is enhanced while the saturation magnetization, M_S, is reduced, (ii) both the 'in-plane' anisotropy field, H_K, as well as the FMR line-width scale with M_S, (iii) the single-ion anisotropy of spin–orbit plus crystal field origin dominates over the two-ion anisotropy of dipolar origin and (iv) multi-magnon scattering contributions to FMR line-width become important in some cases.

Keywords. Ferromagnetic resonance; nanocrystalline soft magnetic alloys; spin-waves; magnetocrystalline anisotropy; line-width.

PACS Nos 76.50.+g; 75.50.Tt; 75.75.+a; 75.30.Ds

1. Introduction

The experimental studies [1–3] of nanocrystalline soft magnetic FeCuNbSiB alloys reported so far have mainly concentrated on the role of grain size in affecting magnetic hysteresis loop parameters, magnetic anisotropy and magnetostriction at room temperature. These studies have indicated that the magnetic softening in the nanocrystalline state occurs because the structural correlation length or grain size becomes smaller than the ferromagnetic exchange correlation length (which is of the order of the domain wall width) with the result that the local random anisotropy is averaged out by the exchange interaction. The present ferromagnetic resonance study aims at obtaining the crucial information about the effect of nanocrystallization on the spin-wave excitations, ferromagnetic relaxation and the temperature dependence of the 'in-plane' anisotropy field, with the amorphous state taken as a reference.

2. Experimental details

Amorphous FeCuNbSiB alloys with actual composition displayed in table 1 (henceforth designated by their Fe concentration, which ranges from 73.26 at% to 74.78

Table 1. Actual composition, saturation magnetization ($M(0,H)$), spin-wave stiffness at 0 K ($D(0)$) and its thermal renormalization coefficient (D_2).

Fe (at%)	Cu (at%)	Nb (at%)	Si (at%)	B (at%)	$M(0,H)$ (G)		$D(0)$ (meV Å^2)		D_2 (10^{-6} K^2)	
					Amor.	Nano	Amor.	Nano	Amor.	Nano
73.26	0.95	3.00	13.08	9.70	1022(6)	1013(2)	109(2)	122(3)	0.75(7)	0.88(8)
73.28	0.94	2.97	15.45	7.36	1125(8)	1030(5)	95(5)	128(5)	2.3(3)	2.1(3)
74.00	1.00	3.00	15.80	6.20	1104(6)	1056(4)	104(5)	135(5)	2.4(5)	2.6(3)
74.37	0.95	3.02	14.15	7.50	1162(4)	1139(7)	90(2)	106(6)	1.0(4)	1.3(3)
74.60	1.00	3.00	15.00	6.40	1169(8)	1110(9)	80(4)	110(10)	1.4(3)	2.1(6)
74.78	0.92	2.63	15.30	6.30	1124(8)	1072(2)	90(3)	109(2)	1.1(2)	0.04(1)

at%) were synthesized by the single-roller melt-quenching technique. They were subjected to annealing at 520°C for 30 min to grow nanocrystals within the amorphous matrix. Amorphous and nanocrystalline counterparts were thoroughly characterized by X-ray diffraction (XRD), scanning electron microscopy (SEM) and the energy dispersive absorption of X-rays (EDAX) techniques. Extensive X-band ferromagnetic resonance measurements have been carried out on these alloys before and after nanocrystallization in the temperature range 100 K to 350 K with a view to clearly bring out the characteristic attributes of the samples in the nanocrystalline state. In this paper, we treat the results obtained on the compositions $Fe_{73.26}$ and $Fe_{74.37}$ as illustrative examples.

3. Results and discussion

Typical room-temperature XRD patterns for the sample $Fe_{74.37}$ and SEM micrograph for $Fe_{73.26}$ in the amorphous and nanocrystalline states are shown in figure 1. The Bragg peaks at $2\theta_B \approx 14°$ and 17° can be unambiguously identified with the (1 1 0) reflection of the tetragonal Fe_3B phase and (0 0 1) reflection of the hexagonal Fe_2Si phase, respectively. The peaks at higher angles can also be indexed, as shown in the figure. Detailed analysis of the XRD patterns using the Scherrer formula, $t = 0.9\lambda/B\cos\theta_B$, together with the SEM and EDAX examination of the nanocrystalline samples revealed Fe_2Si (Fe_3B) nanocrystals of average size 25 nm (30 nm), embedded in an amorphous matrix, which had become poorer in Fe content after nanocrystallization.

An elaborate line-shape analysis (whose details are given in our earlier publications [4,5]) of the resonant microwave power absorption derivative (dP/dH) vs. static magnetic field (H) spectra taken at fixed temperatures in the range 100 K to 350 K on rectangular strips of dimensions $4\times2\times0.03$ mm^3 in the horizontal-parallel ($\|^h$) and vertical parallel ($\|^v$) sample configurations, yielded accurate values for the Landé splitting factor (g), saturation magnetization ($M_S \equiv M(T,H)$), resonance field (H_{res}), 'in-plane' uniaxial anisotropy field ($H_K = [H_{res}(\|^v) - H_{res}(\|^h)]/2$), and 'peak-to-peak' ferromagnetic resonance (FMR) line-width (ΔH_{pp}), at different

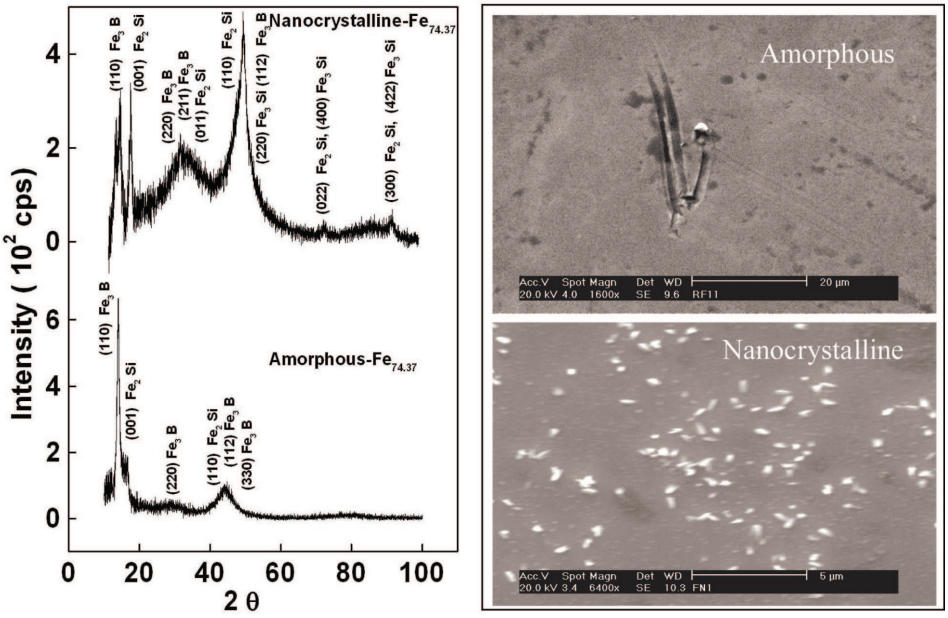

Figure 1. Room-temperature X-ray diffraction patterns for $Fe_{74.37}$ and SEM micrographs for $Fe_{73.26}$ in the amorphous and nanocrystalline states.

temperatures. In the $\|^{\mathrm{h}}(\|^{\mathrm{v}})$ sample geometry, H lies in the ribbon plane and is directed along the length (breadth). Figure 2 displays the M_{S} vs. $T^{3/2}$ plots and the optimum theoretical fits (continuous curves) to the M_{S} (T) data (symbols) based on the well-known spin-wave expression [6,7]

$$M(T,H) = M(0,H) - g\mu_{\mathrm{B}} Z\left(\frac{3}{2}, t_H\right)\left[\frac{k_{\mathrm{B}}T}{4\pi D(T)}\right]^{3/2} \tag{1}$$

with

$$D(T) = D(0)(1 - D_2 T^2). \tag{2}$$

In eq. (1), the Bose–Einstein integral function $Z(3/2, t_H) = \sum_{n=1}^{\infty} n^{-3/2} \exp(-n\, t_H)$ with $t_H = T_{\mathrm{g}}/T = g\mu_{\mathrm{B}}\, H_{\mathrm{eff}}/k_{\mathrm{B}}T$, allows for the extra energy gap $g\mu_{\mathrm{B}}H_{\mathrm{eff}} = k_{\mathrm{B}}T_{\mathrm{g}}$ in the spin-wave spectrum arising from the effective field $H_{\mathrm{eff}} = H - 4\pi NM + H_K$, where N, M and H_K are the demagnetizing factor, magnetization and anisotropy field, respectively. The best fits to the $M_{\mathrm{S}}(T)$ data based on eqs (1) and (2) yield values for the spin-wave stiffness at 0 K $(D(0))$, the coefficient of the T^2 term in eq. (2), (D_2), and $M(0,H)$, as displayed in table 1. It is noticed from the entries in table 1 that an enhancement in $D(0)$ upon nanocrystallization is associated with a reduction in $M(0,H)$. Note that the spin-wave stiffness renormalizes with temperature in accordance with the relation predicted by the itinerant-electron model, i.e., eq. (2), but the same is not true for the relation $D(T) = D(0)(1 - D_{5/2}T^{5/2})$, predicted by the localized electron model

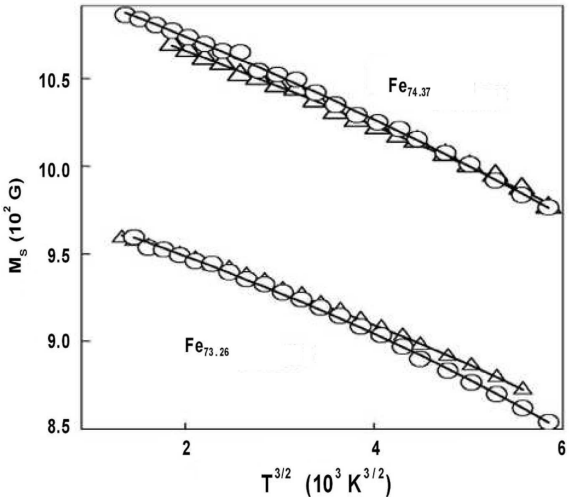

Figure 2. M_S vs. $T^{3/2}$ plots. The symbols open circles (amorphous) and open triangles (nanocrystalline) represent the data while the continuous curves denote the best least-square fits based on eqs (1) and (2).

[7]. H_K either depends on temperature or is constant, H_K^0, over a certain temperature range. In the temperature range where H_K decreases with increasing temperature, $H_K(T)$ scales with $M_S(T)$, as is evident from figure 3. In view of the relation $H_K = 2K_\mathrm{u}/M_\mathrm{S}$ between H_K and the uniaxial anisotropy constant K_u, a linear dependence (no dependence) of H_K on M_S, i.e., $H_K = a + bM_\mathrm{S}$ ($H_K = c$), reflects the fact that $K_\mathrm{u}(T) = [aM_\mathrm{S}(T) + bM_\mathrm{S}^2(T)]/2$ ($K_\mathrm{u}(T) = (c/2)M_\mathrm{S}(T)$). These relations thus permit the computation of $K_\mathrm{u}(T)$ and reveal that the anisotropy is predominantly of the single-ion type (arising basically from the combination of spin–orbit interaction and crystal field effects). The values of K_u at room temperature, so determined, for various compositions conform very well in magnitude with those reported for similar nanocrystalline systems in the literature.

Figure 4 demonstrates that ΔH_pp is related to M_S as

$$\Delta H_\mathrm{pp} = \Delta H_0 + a' M_\mathrm{S}(T) + b' M_\mathrm{S}^2(T), \tag{3}$$

where ΔH_0 is the intrinsic FMR line-width whereas the second and third terms in eq. (3) represent contributions to ΔH_pp arising from two-magnon and multi-magnon scattering caused by spatial inhomogeneities in the local magnetic anisotropy fields and/or inhomogeneities in the local exchange interaction; the third term turns out to be important only in the case of nanocrystalline $Fe_{73.28}$ and $Fe_{74.37}$ alloys. Note that the alloys $Fe_{73.26}$ and $Fe_{73.28}$ widely differ in the concentration of elements other than Fe (see table 1). The main finding, based on eq. (3), is that upon nanocrystallization, the intrinsic line-width ΔH_0 reduces by a factor of two while the coefficient a' of the second term remains practically unaltered.

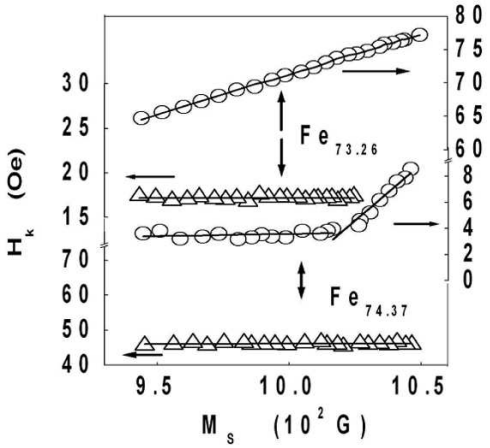

Figure 3. Scaling of H_K with M_S in the amorphous (open circles) and nanocrystalline (open triangles) counterparts. Note the break between different ordinate scales.

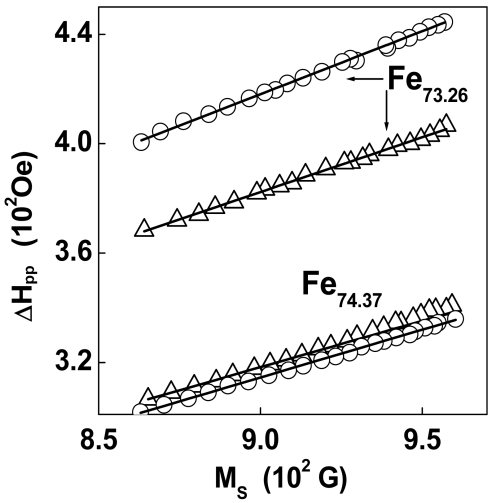

Figure 4. Scaling of $\Delta H_{\rm pp}$ with M_S in the amorphous (open circles) and nanocrystalline (open triangles) counterparts.

4. Conclusions

The results of the present investigation permit us to draw the following conclusions concerning the characteristic attributes of the FeCuNbSiB magnetic alloys in the nanocrystalline state.

- Spin-wave stiffness (D) is enhanced while the saturation magnetization (M_S) is reduced.

- The 'in-plane' anisotropy field (H_K) has a constant value, which depends on composition. However, in certain cases, $H_K(T) \propto M_S(T)$ in specific composition-dependent temperature ranges.
- The FMR line-width scales with M_S for all the compositions.
- Compared to the value in the amorphous state, the intrinsic FMR line-width is reduced by a factor of two in the nanocrystalline state.
- The single-ion anisotropy, arising from the combined effect of the spin–orbit interaction and crystal field, dominates over the two-ion anisotropy of dipolar origin.
- Multi-magnon scattering contributions to FMR line-width become important in some cases.

Acknowledgments

This work was supported by the Department of Science and Technology, New Delhi, through grant No. SR/S5/NM-04/2003.

References

[1] G Herzer, in: *Handbook of magnetic materials* edited by K H J Buschow (Elsevier, Amsterdam, 1997) vol. 10, p. 415
[2] D S Schmool and J M Barandiarán, *J. Magn. Magn. Mater.* **191**, 211 (1999)
[3] M Müller, N Mattern and L Illgen, *J. Magn. Magn. Mater.* **112**, 263 (1992)
[4] S N Kaul and V Siruguri, *J. Phys.: Condens. Matter* **4**, 505 (1992)
[5] V Siruguri and S N Kaul, *J. Phys.: Condens. Matter* **8**, 4545, 4567 (1996)
[6] S N Kaul, *J. Phys.: Condens. Matter* **3**, 4027 (1991)
[7] S N Kaul and P D Babu, *J. Phys.: Condens. Matter* **4**, 6429 (1992)